Title

Assessment of mechanical properties and microstructure characterizing techniques in their ability to quantify amount of cold work in 316l alloy

Journal

Journal of Engineering Materials and Technology, Transactions of the ASME, 142(4)

ISSN

0094-4289

Authors

Smith, H
Linke, BS
Muránsky, O
et al.

Publication Date

2020-10-01

DOI

10.1115/1.4047024

Peer reviewed

Assessment of mechanical properties and microstructure characterizing techniques in their ability to quantify amount of cold work in 316L alloy

Submitted to ASME Transactions J. Eng. Mater. Technol.
Original submission Sep 2019; Accepted in revised form Apr 2020
Available at https://doi.org/10.1115/1.4047024

Authors:

Helen Smith, Mechanical and Aerospace Engineering, University of California Davis, now at Sandia National Laboratory, Livermore, CA

Barbara S. Linke*, Mechanical and Aerospace Engineering, University of California Davis

Ondrej Muránsky, Australian Nuclear Science and Technology Organisation, ANSTO, Australia

Cory Hamelin, Australian Nuclear Science and Technology Organisation, ANSTO, Australia, now at EDF Energy, UK

Michael R. Hill, Mechanical and Aerospace Engineering, University of California Davis

*Corresponding author

ABSTRACT

Stress corrosion cracking (SCC) behavior is a matter of concern for structural materials, namely stainless steels and nickel alloys, in nuclear power plants. High levels of cold work (CW) have shown to both reduce crack initiation times and increase crack growth rates. Cold working has numerous effects on a material, including changes in microstructure, mechanical properties, and residual stress state, yet is typically reported as a simple percent change in geometry. There is need to develop a strategy for quantitative assessment of cold work level in order to better understand stress corrosion cracking test data. Five assessment techniques, commonly performed alongside stress corrosion cracking testing (optical microscopy, electron backscatter diffraction, X-ray diffraction, tensile testing, and hardness testing) are evaluated with respect to their ability to quantify the level of CW in a component. The test material is stainless steel 316L that has been cold-rolled to three conditions: 0%, 20%, and 30% CW. Measurement results for each assessment method include correlation with CW condition and repeatability data. Measured values showed significant spatial variation, illustrating that CW level is not uniform throughout a component. Mechanical properties (tensile testing, hardness) were found to correlate most linearly with the amount of imparted CW.

1 INTRODUCTION

Cold work (CW) is an important consideration in the operation and maintenance of nuclear power plants. In order to relicense plants for extended operation, the Nuclear Power industry evaluates reactor internals components using specific guidelines, generic component listings and

screening criteria that includes cold work level as defined in Materials Reliability Program MRP-175[1,2,3]. These guidelines consider fabrication, forming, and finishing processes, and screen for "severe cold work", which is defined as 20% CW or greater. 20% CW is the evaluation limit, that is, intentionally cold-worked components must have less than 20% CW. Current engineering controls during fabrication consist of limiting material yield strength to ensure compliance with this 20% threshold [4]. Cold work is of particular concern because of its effect on stress corrosion cracking (SCC) behavior. High levels of cold work exacerbate SCC behavior, and have been shown to increase crack growth rates (CGR) [5,6, 7] and reduce crack initiation times (CIT) [8, 9]. However, the specific mechanisms by which cold work affects SCC behavior are still unclear [1, 9] and further investigation is needed to understand the implications of laboratory test data on expected material performance in operating plants.

Cold working, also known as strain or work hardening, is the process of plastic deformation performed significantly below recrystallization temperature. Work hardening affects several material properties, making CW level difficult to define and measure quantitatively. In practice, CW is reported as a relative change in one or a number of orthogonal dimensions [10]; when applied to rolling of flat plates for example, this corresponds to percent thickness reduction. Percent cold work (%CW) is a solely geometric parameter, and thus fails to take into account elasto-plastic material properties, microstructure, residual stress state, and any inhomogeneity/anisotropy present in the material. Furthermore, the reported %CW does not provide any information about the process itself. In the context of SCC performance, the measure of relative change in one or a number of overall dimensions does not provide any real insights into the consequence of CW on SCC [9, 11, 12]. Consider the Bettis lab data set presented in [13]: Crack growth rates observed in 24% cold-rolled Inconel alloy 690 were an order of magnitude higher than those observed in 31% tensile pre-strained material from the same heat lot.

The complex nature of the relationship between CW and SCC behavior in stainless steels and nickel alloys is well documented, although the way that CW affects crack growth rate is still unclear [12, 14]. For SCC to occur, three conditions must exist and interact in a synergistic way: (i) susceptible material, (ii) corrosive environment, and (iii) tensile stress state [11]. When a material is cold-worked, the changes in macroscopic overall dimensions (geometry) are accompanied by a number of microstructural changes (dislocations, grain size), and a change in stress state due to introduction of residual stresses. The overlap in effects from cold-working and conditions necessary for SCC occurrence makes it difficult to identify a single parameter that accurately predicts SCC performance [9, 14].

Quantifying CW level in a robust, repeatable way is critical for designing, manufacturing, and maintaining nuclear power plants because it will allow for more accurate comparison between laboratory test data and conditions found in plant components. Test data for stress corrosion cracking behavior of plant materials is often derived from coupons containing high levels of cold work [6, 13, 15]. Plant components are fabricated using methods that typically impart far lower levels of cold work [3, 4, 16]. Engineering work, test methods, guidance, and specifications are needed to characterize the level of cold work in reactor materials in order to enable test data from highly cold worked materials to be used for accurate forecasts of plant performance. This need is especially important because some plant materials exhibit a large decrease in stress corrosion cracking resistance beyond a threshold level of cold work [4], and

the cold work levels in test materials and plant components are very often on opposite sides of this threshold.

A variety of experimental techniques have been used in assessment of CW alongside SCC testing. These include: electron backscatter diffraction (EBSD) maps and calculated Kernel Average Misorientation (KAM) values, broadening of X-ray diffraction peaks, microhardness, yield strength, residual stress measurement, transmission electron microscopy (TEM) scans, and others [16, 17,18,19]. Although investigations of SCC behavior in cold-worked materials often include more than one of these techniques [13, 20, 21, 22], there has not yet been a rigorous comparison between these techniques. The primary objective of this work is to examine and compare common assessments of CW with respect to their ability to quantify the level of CW in a component. For simplicity, the focus is on quantifying CW effects on the material itself, not including water chemistry or stress state, even though all three affect SCC behavior.

Five CW assessment methods are identified and applied to test material. Results from each method are evaluated separately and together in order to generate a set of preliminary guidelines for CW characterization. By first analyzing several methods in a laboratory setting on test material with simple coupon geometry, quantitative assessment methods, such as microstructural evaluation, mechanical testing, and residual stress measurement, can be correlated with observed %CW, and a robust characterization can eventually be obtained. Such a characterization methodology can then be applied to both test material and plant components in order to better understand and predict SCC behavior.

2 EXPERIMENTAL

2.1 Material

The present study was conducted on a set of 316L plates, all cut from a single heat (610344-3A), obtained from American Stainless Corp (composition given in Table 1). The main phase in this grade of steel is austenite. Small amounts of δ-ferrite are often present in this grade of stainless steel, allowing for easier hot machinability by providing resistance to cracking at elevated temperatures [23]. Construction of a Schaeffler diagram based on the test material chemical composition predicted the presence of 6% δ-ferrite (this was later confirmed using employed experimental techniques). Two plates, 127 mm x 355.6 mm x 25.4 mm, were uni-directionally cold rolled to levels of 20% and 30% thickness reduction. A third plate of the same material and dimensions was kept in as-received condition before cold working, and shall be referred to as the 0% or unworked condition. All plates were hot rolled, annealed and pickled per ASME SA-240 before cold working. Figure 1 shows the orientation and layout of test specimens in a plate. A number of different samples were extracted from each plate using wire electric discharge machining (EDM) in order to minimize stress and deformation from cutting. The three primary axes - rolling direction (RD), transverse direction (TD), and normal direction (ND) - are labeled in Figure 1. All planes of interest throughout the paper are specified by the two in-plane axes. Thickness is abbreviated with symbol t.

2.2 Mechanical properties testing

2.2.1 Tensile testing

In order to assess changes in mechanical strength properties, four round tensile samples with a 0.350 in (8.89 mm) gauge diameter were tested from each plate, two in the RD and two in the TD. The sample location can be seen in Figure 1. Testing samples in both orthogonal directions

allows investigation of directional dependence of mechanical properties. Stress-strain flow curves were generated to fracture per ASTM E8/E8M-13a [24]. Both yield strength (YS) and ultimate tensile strength (UTS) are extracted from the generated stress-strain curves. These properties, instead of others available from tensile testing (ductility, toughness, etc.) were chosen for evaluation because of their reported correlation with SCC behavior [9].

2.2.2 Rockwell hardness

Rockwell hardness measurements were carried out on a total of three 19.05 x 8.9 x t mm samples oriented in the RD-ND plane (one sample per CW condition). This sample geometry was chosen to be consistent with the samples used for optical microscopy and X-ray diffraction. Tests were conducted on a Buehler Macromet Rockwell Hardness tester per ASTM E18-14a [25]. Five replicate measurements were taken per sample, all located at t/2 location (half thickness). Increases in material hardness from the unworked to worked conditions required the collection of hardness measurements on two different scales. For the 0% sample the measurements were collected using the B scale, and for the 20% and 30% samples measurements were taken using the C scale. These scales were chosen by following recommendations outlined in ASTM E18-14a. In order to compare hardness between all CW conditions, measurements were converted and reported on the A scale, using the appropriate conversions tables found in ASTM E140 [26].

2.3 Microstructural examination

In addition to tensile and hardness testing we employed three microstructure characterizing techniques: (i) optical microscopy, (ii) electron backscatter diffraction (EBSD), and (iii) X-ray diffraction (XRD). While all of these techniques provide information about the microstructure, the properties that they measure are inherently different. Optical microscopy provides qualitative characterization of grain size and shape, material phases (austenite, ferrite), and microstructural features (twin boundaries, etc.), and quantifies grain size and shape in one plane. EBSD provides both qualitative and quantitative information about crystallographic orientation. Analysis of EBSD orientation maps can provide a measure of geometrically necessary dislocations (GNDs), while EBSD measurement is insensitive to the presence of statistically stored dislocations (SSDs). XRD peak broadening is a quantitative measure that corresponds to microstrains in the crystal lattice caused by the presence of GNDs and SSDs – hence XRD peak broadening analysis can provide total dislocation density.

2.3.1 Optical Microscopy (OM)

Several micrographs were collected at both the surface and mid-thickness of the plate to account for microstructural variation through the thickness. Nine metallographic samples were prepared in total in order to observe the microstructure in all three orthogonal directions. One sample from each plane (RD-ND, TD-ND, RD-TD) was extracted from each plate. The sample dimensions are 19.05 x 8.9 x t/2 mm. This sample geometry was chosen with expectation of symmetry about the mid-thickness. Full thickness samples were not advantageous due to restrictions in polishing apparatus and microscope stage limitations. The RD-TD sample plane was located at t/2 to avoid shallow work-hardening effects near the surface.

Samples were mounted in resin and polished automatically with protocols shown in Table 2 in order to obtain consistent surface finishes. Polished samples were subsequently etched by swabbing 30s with aqua regia [27] to observe general microstructural features as well as grain

boundaries. After etching, several photomicrographs were collected as grayscale images in an optical microscope under bright-field illumination. As per the ASTM E112-13 [28], grain size and shape were determined using the Heyn lineal intercept method with all six directed test lines. Grain size/shape measurements are only performed at mid-thickness. Micrographs were taken at 200x magnification and four fields were analyzed per sample, with about 100 grains per field.

From these micrographs, the average lineal length in each of the principle directions is tabulated. This corresponds to the average length of grain in a particular direction. Calculation of traditional grain size is not attempted because the grains are expected to be heavily distorted, and ASTM does not recommend grain size calculation in heavily cold-worked materials. To assess repeatability, the standard deviation in average lineal length is calculated from the lineal lengths determined in each field. In order to quantify grain shape, the Anisotropy Index (AI), defined in ASTM E112-13 as the ratio of the average lineal lengths, is tabulated as well.

2.3.2 Electron Backscatter Diffraction (EBSD)

Twelve samples were extracted for EBSD measurements using EDM machining to prevent plastic deformation during sample extraction. Samples were extracted from each orthogonal plane, one from each of the TD-ND and RD-ND planes, and two from the TD-RD plane. Two scans were taken on each of the TD-ND and RD-ND samples, one within 1mm of the surface and one within 1mm of the mid-thickness to investigate through-thickness variation. The samples extracted from the TD-RD plane were located at t/2 and at t/4. This ensures EBSD measurements account for both surface and bulk effects. Sample size and orientation as well as approximate scan locations are shown for a typical plate in Figure 2.

Since high quality surface preparation is required for EBSD in general, and EBSD-based KAM analysis specifically, samples were polished using the following steps: rough surface grinding, fine surface grinding, multi-stage mechanical polishing, fine mechanical polishing, and finally electropolishing (see Table 3). EBSD measurements were taken with a scanning electron microscope at 150x magnification, 20 kV, 60 μm aperture, and 70° stage tilt. The scan area was 300 x 300 μm^2, with step size 0.2 μm, 4x4 binning. Since noisy experimental data leads to overestimating of the imparted plastic strain, it is a common practice to apply a de-noising of the data before further analysis of the data. Therefore, an averaging filter[1] was applied to each measurement points (pixel) in EBSD orientation maps in order to minimize the error in the measured crystal orientations.

Traditionally, Kernel Average Misorientation (KAM) is calculated as an average crystallographic misorientation angle in a kernel of pixels, between the central pixel in the kernel (p_0) and its four immediate neighboring pixels ($p_i^{(1)}$).

$$M_L^{(1)}(p_0) = \frac{1}{4}\sum_{i=1}^{4} \beta(p_0, p_i^{(1)}) \tag{1}$$

where $\beta(p_0,p_i^{(1)})$ is the angular misorientation between p_0 and $p_i^{(1)}$. Provided a constant lattice curvature exists within the kernel, greater accuracy in KAM calculations will result from an extended misorientation analysis, where the kernel is extended to include surrounding pixels p_i

[1] The average of the crystal orientations of surrounding pixels is calculated (provided the neighboring pixels occupy the same grain), and the original orientation measured at a given pixel is updated with the averaged value. A nine-pixel (3 × 3) filter was used, thereby considering the additional data from up to eight neighboring pixels.

that are not necessarily adjacent to p_0 (only including the neighboring pixels that occupy the same grain). In the present work, KAM $M_L^{(5)}$ is calculated for each scan area. This extended KAM is calculated using pixels $p_i^{(5)}$, which are located a distance of $h_0\sqrt{8}$ from p_0 (where h_0 is the EBSD step size, 0.2 μm).

$$M_L^{(5)}(p_0) = \frac{1}{4}\sum_{i=1}^{4} \beta(p_0, p_i^{(5)}) \tag{2}$$

Once an extended KAM analysis of all pixels within an EBSD scan area is complete, the mean and variance of the KAM for this area is obtained by assuming a log-normal misorientation distribution.

$$f(x|\mu,\sigma) = \frac{1}{x\sigma\sqrt{2\pi}} \exp\left\{\frac{-(\ln(x)-\mu)^2}{2\sigma^2}\right\} c \tag{3}$$

where the mean (m) and variance (v) are defined as follows:

$$m = \exp\left\{\mu + \frac{\sigma^2}{2}\right\} \tag{4}$$

$$v = \{2\mu + \sigma^2\}\{\exp(\sigma^2) - 1\} \tag{5}$$

Volume fraction of deformation twins in the cold-worked samples is also extracted from the EBSD orientation maps. To accomplish this, deformation twins were identified as either grains with high aspect ratio and/or small area relative to the parent grains. Using this threshold criteria, most of the deformation twins can be successfully identified, and volume fraction is reported.

We estimated the volume fraction of twins based on the misorientation relationship between the parent and twin grains. This was supposed to provide an estimate.

2.3.3 Peak broadening (X-ray diffraction)

Several studies show strong correlation between cold work percentage and peak width in X-ray diffraction profiles for both steels and nickel based alloys [29, 30, 31]. In this study the (200) peak was examined because it shows detectable broadening for steel [18]. The (200) reflection is affected by the strain broadening similar to other reflections: (220) and (222) [32]. Nine samples (19.05 mm x 8.9 mm x t/2 mm) were taken from each plate for a total of 27 samples. Three replicates from each orthogonal direction (per plate) were included to facilitate study of repeatability within each plane and CW condition. The samples were mounted in resin and polished in the same manner as the OM samples in order to remove the wire EDM surface. Once sufficiently prepared (see protocols in Table 2), each sample was scanned over a 48-54 °2θ range to capture the 200 peak. Scans were conducted on a Panalytical X'Pert Pro MRD diffractometer with Bragg-Brentano geometry and CuKα target at 45 kV, 40 mA. A fixed divergence slit of 1°, 10 mm mask, fixed receiving slit of 1°, step size of 0.02 °2θ, and dwell time of 0.5 s were used for all scans. Intensity profiles were detected using Panalytical commercial software and then exported for further analysis.

Pearson VII shape functions, which range from Cauchy to Gaussian distributions, were fit to the experimental profiles using non-linear least squares as outlined by Prevéy [29]. The total

intensity profile can be represented as the sum of the $K\alpha_1$ and $K\alpha_2$ doublet plus a linear background. The ratio of peak intensities for $K\alpha_1$ and $K\alpha_2$ is held at 0.5, and the wavelengths are λ_1 = 1.540598 Å, λ_2 = 1.544426 Å, respectively. Peak width is reported as the calculated full width at half maximum (FWHM) of the α_1 peak in order to avoid any broadening due to doublet separation. No corrections for instrumental broadening were applied, as this broadening is assumed constant over the small 2θ range scanned to capture the 200 peak. Due to the large grain size of the alloy the broadening due to crystallite size effects is assumed negligible and not corrected for. Plastic anisotropy is not taken into account.

After calculating FWHM for each sample, the average peak width and standard deviation are calculated for each plane and CW condition to assess repeatability between orthogonal planes. The overall average and standard deviation for each CW condition (calculated from all three planes) is also reported and then compared with %CW due to rolling.

3 RESULTS

3.1 Mechanical Properties

3.1.1 Tensile strength

Yield strength (YS) and ultimate tensile strength (YTS) were obtained from tensile testing for all tested samples. Figure 3 shows stress-strain curves for one sample from each CW condition. As expected, work hardening is readily apparent as CW condition increases. Figure 4 and Figure 5 show YS and UTS as a function of CW condition, respectively. Note that YS, and UTS have been identified as factors influencing SCC behavior [9]. The YS in the transverse direction is consistently higher than the strength in the RD for the worked conditions, and similar to the RD for the 0% condition. The same trend is seen for the UTS. There are clear increases in both YS and UTS between 0%, 20%, and 30% conditions, and the precision (reported as one standard deviation) is sufficient to distinguish between the three conditions.

3.1.2 Rockwell hardness

Tabulated values for Rockwell hardness on measured scales and converted “A” scale are presented in Table 4. Like the strength properties found from tensile testing, hardness values increase significantly with each CW condition. The “A” scale values are plotted vs. CW condition (Figure 6). The trend with %CW appears linear (with the reservation that only few points are examined), similarly to the trend for YS and UTS. Precision is reported as one standard deviation (error bars on plot), and is sufficient to differentiate among the CW conditions.

3.2 Microstructure

3.2.1 Optical microscopy

As expected, optical micrographs showed significant through-thickness variation in microstructure for all CW conditions. For the 0% condition, Figure 7 shows optical micrographs in the TD-ND plane taken at thickness t/2 and adjacent to the surface. There are mainly equiaxed grains near the plate mid-thickness, while elongated grains are found near the surface - this is consistent with dynamic recrystallization at the surface during initial hot-rolling, with large grains remaining after annealing. This zone of elongated grains extends approximately t/10 from each rolled surface. Figure 8 presents of optical micrographs taken at mid-thickness for each of the three orthogonal planes in each cold-worked condition. With an increasing amount of CW,

grains elongate in the RD and deformation twins are observed. Grain elongation and emergence of deformation twins are most clearly visible in the RD-ND orientation. There appears to be a higher fraction of deformation twins as the level of cold-work increases from 20% to 30%. Several dark stringers are also observed along RD in the RD-ND plane – these were identified as δ-ferrite.

Grain size and shape for each CW condition were calculated from optical micrographs taken at mid-thickness. When comparing the 0% and 20% conditions, there is clear lengthening of the grains in the RD and shortening of grains in the ND, while TD remains roughly unchanged. This can be observed in both the average lineal lengths and the anisotropy indices. However, the difference between 20% and 30% is less distinct, and not significant once the precision is taken into account. Average lineal lengths are plotted in Figure 9 in order to visualize their trend.

3.2.2 EBSD

Table 5 lists relevant statistics from every EBSD scan, including the indexing rate, the average Mean Angular Deviation (MAD) and the number of analyzed grains. Both the indexing rate and the MAD are useful when determining the accuracy of EBSD orientation measurements. The indexing rate measures the fraction of indexed pixels captured in each scan, while the MAD (in degrees) measures the angular misfit between detected and simulated Kikuchi bands. Both values are affected by the level of accumulated plastic strain in the specimen (i.e. amount of CW), but may be influenced by the surface preparation. The lower bound indexing rate for the scans presented in Table 5 is 81.0 percent, which infers a high degree of confidence in the collected EBSD data and subsequent KAM analyses.

Figure 10 presents a scan for the 0% condition as an example of EBSD data collected. Data is presented in two forms: (i) an orientation map, useful for phase identification, texture studies, and grain statistics; and (ii) a KAM map, useful for determining the amount of plastic deformation accommodated by GNDs forming substructure that exists within each grain. In the EBSD orientation maps, the delta-ferrite was unindexed (white) and was thus omitted from the further analysis. Note that there is also a low fraction of unindexed austenite pixels in region of high plastic deformation, e.g. at grain boundaries. From the KAM map set of information, the mean KAM is calculated. The KAM for each scan area is calculated by finding the mean from a log-normal distribution function, and mean KAM values for each scan are listed in Table 5. Figure 11 and Figure 12 show KAM and twin volume fraction as a function of CW condition, respectively. There is a distinct difference in behavior between results collected near the surface and results collected near mid-thickness for both of these values. In general, KAM increases significantly with CW level, with distinct differences with %CW, although the trend is not linear. KAM vs %CW trends are somewhat similar for surface and mid-thickness scans, although the difference between 20% and 30% is less pronounced, and there is more variability in the measurement. Twin volume fraction near mid-thickness shows increasing density of deformation twins with increasing CW level, with the biggest increase occurring between 20% and 30% CW. Surface twin volume fraction shows no significant difference between 20% and 30%, and has significantly more spread in measured values. Note that no deformation twins were observed in the 0% condition, although annealing twins are present, as can be seen in Figure 7.

3.2.3 XRD peak broadening

An example fit of a Pearson VII function to experimental XRD intensity data is shown in Figure 13. Contributions from the linear background, $K\alpha_1$, and $K\alpha_2$ components add linearly to fit the experimental data. Full Width at Half Maxima of {200} diffraction peak is determined from the α_1 component. Scans from different sample orientations are averaged - it is reasonable to average scans from different planes because a large volume of material is being probed. Furthermore, no significant or systematic differences between planes were observed. Figure 14 shows the average FWHM from all nine samples as a function of %CW. There is a clear increase in peak width from 0% to 30%, but from 20% to 30% the increase is not statistically significant.

4 DISCUSSION

Both tensile and hardness properties were similar, with nearly linear correlation with %CW and good repeatability. Compared to Rockwell hardness, tensile testing is advantageous because it provides multiple strength properties in a single test, it shows directional anisotropy, and is inherently more a bulk or average measure. However, Rockwell hardness measurement requires far less material, and can assess spatial variation of condition. With regard to the microstructure characterizing techniques, no single technique appears sufficient to characterize microstructure fully. OM was the quickest, easiest way to get a qualitative sense of the microstructure and identify microstructural features (such as twins and ferrite stringers), yet quantitatively it was fairly ineffective, as grain size and shape correlated poorly with %CW. KAM and twin volume fraction from EBSD data correlated well with %CW and take into account presence of dislocation slip and dislocation twinning. However, EBSD only assesses GNDs, not total dislocation density. EBSD is also a localized measure; and can require an order of 10^4 grains to be scanned in order to get a reasonable indication of bulk material condition. Therefore, XRD is an important method to include in addition because it can be used as an assessment of statistically stored dislocations (SSDs), and operates at a bulk scale, as compared to EBSD.

4.1 0% CW condition

Both EBSD and mechanical testing showed that the 0% condition is not necessarily 100% “work-free”. KAM in the 0% condition shows that while some grains have undergone full recrystallization, many grains still possess considerable dislocation substructure due to prior hot rolling. The KAM values in Table 5 show that the as-received material contains some amount of pre-existing plastic deformation, as KAM values around 0.4°are observed when KAM values of about 0.1° degrees are expected for fully recrystallized material [33]. YS measurements also imply that as-received material has some work hardening associated with the 0% condition, as these values are nearly double the minimum yield strength specified in ASTM A240/A240M, being about 350 MPa compared to 170 MPa. The influence of the pre-existing dislocation substructure and increased strength are likely important in studying of the material sensitivity to SCC. It may not be useful to compare %CW across materials and tests if differences in the 0% condition are not accounted for, and nominal material conditions are not carefully specified.

4.2 Correlation with %CW

Several key results are combined in order to compare overall trends directly by normalizing each individual result to its value in the 20% condition (Figure 15). Microstructural and mechanical measurements are offset from one another to facilitate distinction between each trend. Normalizing to the 20% value allows the different methods to be easily compared in both

the 0-20% range and the 20-30% range. YS is only included for one direction (RD) because the TD has consistently higher values, however, the overall trend was the same. UTS is not included because, it too shows the same trend as YS. Grain size is included as average lineal length in the RD for easier comparison due to this being an increasing value.

Mechanical properties are observed to correlate more linearly with the amount of CW than microstructural characteristics. YS has the most linear correlation throughout the entire range of any method, as the slope remains nearly constant from 0% to 30% CW. Hardness has similar behavior, but with a shallower slope. KAM has the steepest slope over the entire range of CW conditions, which implies that it is the most sensitive indicator overall for detecting small changes in %CW. Aside from twin volume fraction, it is also the only metric studied that has a bigger difference between 20% and 30% than between 0% and 20%. XRD has a distinct difference between 0% and 20%, but no significant difference between 20% and 30% - this is caused by annihilation of SSDs at higher strain levels.

4.3 Spatial variation

Significant through-thickness variation was observed in all of the microstructural CW assessments (spatial variations of mechanical properties were not observed here, because the mechanical techniques were only used in the subsurface material). The differences observed in surface and mid-thickness measurements suggest that a single scalar “cold-work” value for an entire component would describe local cold-work levels poorly. Material inhomogeneity (i.e., local variation), alongside the extent of CW, have been identified as primary factors in SCC susceptibility [14]; as such it is necessary for a CW characterization strategy to include assessment of CW spatial variation.

Local variation of a condition is lost when reporting CW level as a scalar value. It is impossible for a scalar to capture the spatial dependence and orientation of measured parameters. But specific spatial distributions of measured values are not easily applied when comparing CW levels of test articles and plant components, with their widely different geometries and processing routes. However, if measurement locations are chosen carefully, local variation can still be accounted for when reporting scalar values. This can be accomplished by understanding clearly the goal of the CW level assessment, including specific locations of interest, and then focusing measures at those locations. A strategy of this kind allows for scalar values that are easy to compare (as opposed to spatial distributions), but local in nature. Consider SCC crack growth rates testing as an example. Test samples are often extracted in the Short transverse/thickness – Longitudinal/rolling (S-L) orientation with the crack located at mid-thickness. In this case, CW assessments (KAM, hardness, etc.) should be performed at mid-thickness, because that is where cracking is occurring. In plant components, CW level characterization should be considered at several locations based upon expected sensitivity to SCC risk, material condition, and operational experience. Such a strategy of focusing on relevant areas of a test piece or plant component would allow a more useful characterization that does not assume a uniform CW level.

4.4 Shortcomings

4.4.1 Rockwell hardness scale

Rockwell hardness measurements were carried out on two different scales, and then compared on a converted A scale. Use of converted hardness values is generally not advisable

because additional error is introduced by using conversion tables. However, hardness values for the 0% condition were better suited to the B scale, and values for the 20% and 30% conditions were better suited to the C scale. Because the trend in hardness matches the trend in strength properties and converted hardness values show distinct differences between each CW condition, the error introduced by converting hardness scales does not appear to have a noticeable effect on the result.

4.4.2 Grain size/shape

Grain size/shape was calculated following ASTM E112-13, but was complicated by the presence of deformation twins. Since twin boundaries are not to be counted, automated methods were difficult to implement because software could not reliably differentiate between twin and grain boundaries in the OM images, so manual counting was used. In order to try and increase precision, an increase of fields from four to five and a doubling of test line lengths were implemented for one orthogonal plane. However, precision improved only slightly, and the considerable additional effort required in counting was not repeated for the other planes. OM may be more useful and reliable in materials that do not exhibit twinning.

4.4.3 EBSD scan orientation

EBSD analysis requires significant time, capital equipment, and rigorous surface preparation to achieve results like those presented here. To reduce the effort required, the number of scans may be reduced. As seen in Table 5, there are no systematic or significant differences observed between measurements from different orthogonal planes. Therefore, effort could be reduced by collecting data from only one plane instead of three orthogonal planes. As already known, in rolled plates, it seems useful to assess the RD-ND plane for evaluation.

4.4.4 XRD scan orientation

Like EBSD, XRD was performed on three orthogonal planes, yet no significant difference between planes was observed. Therefore, peak width analysis on one plane could substitute analyses on planes of different orientation to reduce effort.

4.5 Guidelines

An ideal CW characterization technique or method would correlate with material susceptibility to SCC, be quick, inexpensive, reproducible, non-destructive, and capture anisotropy and spatial non-uniformity. None of the methods studied are perfect, yet each has distinct advantages. Advantages and disadvantages of each method are summarized in Table 6. The rows of the table correspond to each CW assessment method, and the columns list the advantages and disadvantages. All methods were evaluated based on correlation with CW condition, costs associated with the method (e.g., time, material required, equipment), repeatability, and ability to characterize effects due to cold working.

Measures calculated from EBSD, KAM and twin volume fraction (with larger spread), had the strongest correlation with %CW and excellent repeatability. These values also tracked spatial variation in microstructure, and accounted for presence of both dislocation slip and deformation twinning. However, it is impractical to use EBSD as the only microstructural assessment method because of its two main disadvantages: it can only assess GNDs, and it requires several scans to get statistically significant information. To overcome these disadvantages, XRD peak width can be included. XRD is inherently a bulk measure, as it averages over significantly larger amount of material, and it is able to assess total dislocation density. EBSD and XRD cover each other's

disadvantages well, except they are both expensive in terms of time and material preparation. To cut down on the number of scans, optical microscopy can be used not as a quantitative tool, but as a qualitative tool to obtain a general sense of the microstructure, identify microstructural features, and plan EBSD and XRD scan locations based on observed spatial variation.

Both mechanical properties had similar advantages: nearly linear correlation with %CW and high reproducibility. Tensile testing was more advantageous because it is an intrinsically bulk measure and provides multiple properties including strength and ductility. It also tracked orientation anisotropy, but cannot provide information about spatial variation. Thus, when component geometry permits tensile coupons and spatial variation is not important, this method is recommended to assess mechanical strength. In instances where tensile coupons cannot be extracted, or large spatial variation is expected (such as in the heat affected zone of a weld), Rockwell hardness is recommended to assess mechanical properties.

Based on the results presented in this paper, the following guidelines should be kept in mind when assessing the effects of cold working on material condition:

- CW level assessment methods should be applied to *locations of interest* (as determined by the goal of CW assessment), since CW is not uniform throughout a component.
- CW affects a component in several ways. A characterization methodology should include quantifying microstructure and mechanical properties to encapsulate the majority of these effects. Residual stress is another promising area for CW characterization.
- **Microstructure** might be quantified by implementing the assessment methods presented in this work as follows:
    - Use optical microscopy to identify key microstructural features and spatial variations in order to choose intelligent scan locations for EBSD.
    - Use EBSD to measure KAM and twin volume fraction at these locations (on one orthogonal plane) to account for slip, twinning, and GNDs.
    - Use XRD (on one plane) to include a bulk assessment of the microstructure and account for SSDs.
- **Mechanical properties** are best measured by tensile testing when component geometry allows tensile samples to be extracted. Hardness measurements may be used instead for geometries where tensile coupons cannot be reasonably extracted, or where spatial variations in CW effects are expected.

These are general suggestions, and may not be appropriate for all circumstances. For example, if trying simply to characterize a material as either “highly” cold-worked (greater than 20%), or non-worked (around 0%), EBSD scans are likely unnecessary, and XRD peak width would be sufficient in quantifying the microstructure. The specific goals and requirements of the CW characterization should be the ultimate driver in method selection and application.

5 CONCLUSION

Five assessment methods were applied to a set of cold-rolled SS 316 plates with respect to their ability to quantify cold work level. These methods can be broken down into two categories:

microstructure characterizing techniques (optical microscopy, EBSD, and XRD peak width) and mechanical properties characterizing techniques (tensile testing, Rockwell hardness). Measurement results for each technique include correlation with CW condition and repeatability data. Measured values from optical micrographs, and EBSD KAM analysis showed significant spatial variation, illustrating that CW level is not uniform throughout a plate (component) thickness. Mechanical properties (tensile testing, hardness) were found to correlate most linearly with the amount of CW, and KAM was found to be most sensitive to %CW, showing that no one assessment method was ideal. Advantages and disadvantages for each method have been discussed, and a set of general guidelines for characterizing cold work's effect on the material is presented. Although a rigorous characterization methodology is yet to be obtained, results from this paper have provided a good initial step. In future, the findings from a study of this type can then be extended to additional materials, geometries, and deformation processes and then refined until a characterization methodology suitable for complicated reactor components, such as the pressure vessel head, is obtained.

6 ACKNOWLEDGMENTS

Financial support was provided through the Electric Power Research Institute (EPRI), grant on *Manufacturing Induced Strain and Long-Term Material Performance* and we thank Dr. Paul Crooker for his guidance.

We also thank Dr. Michael Burke for the extensive and fruitful discussions, as well as thank you to Akira Nakagawa, Yohei Sakakibara, Takashi Hirano, Teruyoshi Sato, Takanori Kunihiro, in addition to others from IHI Corporation.

7 TABLES

Table 1: Chemical composition of 316L Plates (wt %) obtained from Outokumpu Stainless Plate, Inc.

C	Mn	P	S	Si	Cr	Ni	Co	Cu	Mo	N	Cb	Ti	Al	Sn
.019	1.59	.033	.011	.35	16.46	10.07	.32	.39	2.04	.03	.015	.003	.003	.008

Table 2: Protocol for automated polishing of metallographic samples. Complimentary: samples and platen rotate in same directions. Contra: samples and platen rotate in opposing directions.

Polishing Cloth	**Polishing Media**	**Time (min)**	**Speed (rpm)**	**Force per sample (lbs)**	**Polishing Direction**
Carbimet Paper, 240 Grit	N/A	2:00	250	6	complimentary
Nylon Pad	9-µm diamond suspension	5:00	160	6	contra
Nylon Pad	3-µm diamond suspension	3:00	130	5	complimentary
Microcloth	0.05-µm alumina suspension	2:00	110	6	contra

Table 3: Protocol for surface preparation of EBSD samples

Polishing Step	**Description**
Rough surface grinding	9-µm diamond suspension and lubricant on grinding disc for hardened steels
Fine surface grinding	9-µm diamond suspension and lubricant on grinding disc for softer materials until damage accumulated from rough grinding removed
Multi-stage mechanical polishing	15-µm diamond suspension on hard polishing cloth, gradually lowering polishing force
	3-µm diamond suspension on hard polishing cloth
	1-µm diamond suspension with lubricant on hard polishing cloth
Fine mechanical polishing	Colloidal silica on specifically designed polishing cloth
Electropolishing	Electrolyte mixture: methanol, 2-butanol, perchloric acid. 60 V for 15 seconds

Table 4: Rockwell hardness measurements. 0% condition collected on the 'B' scale; 20% and 30% conditions collected on the 'C' scale. All values converted to the 'A' scale for ease of comparison. Precision uncertainty reported as one standard deviation

%CW	HRB	HRC	(HRA)
0	82.7	--	51.3
	84.3	--	52.3
	84.6	--	52.5
	84.3	--	52.3
	83.3	--	51.7
			52.0 ± 0.502
20	--	23.8	62.2
	--	24.3	62.5
	--	22.1	61.4
	--	22.6	61.6
	--	22.8	61.7
			61.9 ± 0.455
30	--	28.3	64.5
	--	29.1	64.9
	--	28.7	64.7
	--	28.4	64.5
	--	27.7	64.2
			64.6 ± 0.261

Table 5: EBSD scan metrics for all scans. Precision uncertainty reported as one standard deviation. The misorientation angle of 7 degrees was used for the grain reconstruction.

%CW	Scan Location		Indexing Rate (%)	Grains Scanned	Average MAD (deg)	Average KAM (deg)
0	RD-TD	surface	97.8	467	0.50	0.457
		mid-thickness	97.8	555	0.49	0.426
	TD-ND	surface	97.0	597	0.49	0.390
		mid-thickness	99.5	209	0.51	0.712
	RD-ND	surface	95.1	537	0.57	0.325
		mid-thickness	99.4	243	0.45	0.276
	Average	surface	96.6 ± 1.4		0.52 ± 0.04	**0.391 ± 0.066**
		mid-thickness	98.9 ± 0.95		0.48 ± 0.03	**0.471 ± 0.222**
20	RD-TD	surface	91.8	825	0.60	0.994
		mid-thickness	94.1	602	0.59	1.01
	TD-ND	surface	96.6	59	0.52	0.871
		mid-thickness	93.8	888	0.46	1.01
	RD-ND	surface	87.9	467	0.41	1.00
		mid-thickness	90.4	800	0.41	0.992
	Average	surface	92.1 ± 4.4		0.51 ± 0.10	**0.955 ± 0.073**
		mid-thickness	92.8 ± 2.1		0.49 ± 0.09	**1.00 ± 0.010**
30	RD-TD	surface	90.3	783	0.47	1.47
		mid-thickness				
	TD-ND	surface	81.0	590	0.52	1.12
		mid-thickness	83.6	1115	0.46	1.57
	RD-ND	surface	88.6	680	0.40	1.22
		mid-thickness	83.0	1018	0.54	1.59
	Average	surface	86.6 ± 5.0		0.46 ± 0.06	**1.27 ± 0.180**
		mid-thickness	83.3 ± 0.4		0.50 ± 0.06	**1.58 ± 0.014**

Table 6: Advantages and Disadvantages of each CW assessment method.

	Advantages	Disadvantages
Optical Microscopy	• relatively quick, easy, inexpensive to get qualitative picture of microstructure • Identify microstructural features • Identify trends to help plan scan locations	• Difficult to apply automated grain count methods due to twin boundaries • Grain size/shape not helpful as quantitative parameters when compared to %CW
EBSD	• KAM and twin volume fraction take both slip & twinning into account • Good correlation with %CW	• Only assesses GNDs • Need to scan many grains to get realistic "bulk" measure • Sample surface preparation time consuming and critical to method success
XRD Peak width	• Intrinsically bulk measure • Only method analyzed to include any information about SSDs	• Not correlated with %CW beyond 20%
Tensile Testing	• Nearly linear correlation with %CW • Provides several strength properties per test • Intrinsically bulk measure • Easily reproducible: follows international standard	• Requires component geometry conducive to removing tensile test samples • Need to test in multiple directions to include orientation effects
Rockwell Hardness	• Nearly linear correlation with %CW • Good for locations where tensile samples cannot be removed • Easily reproducible: follows international standard	• Indirect measure of strength • Requires several tests to get bulk measurement

8 FIGURES

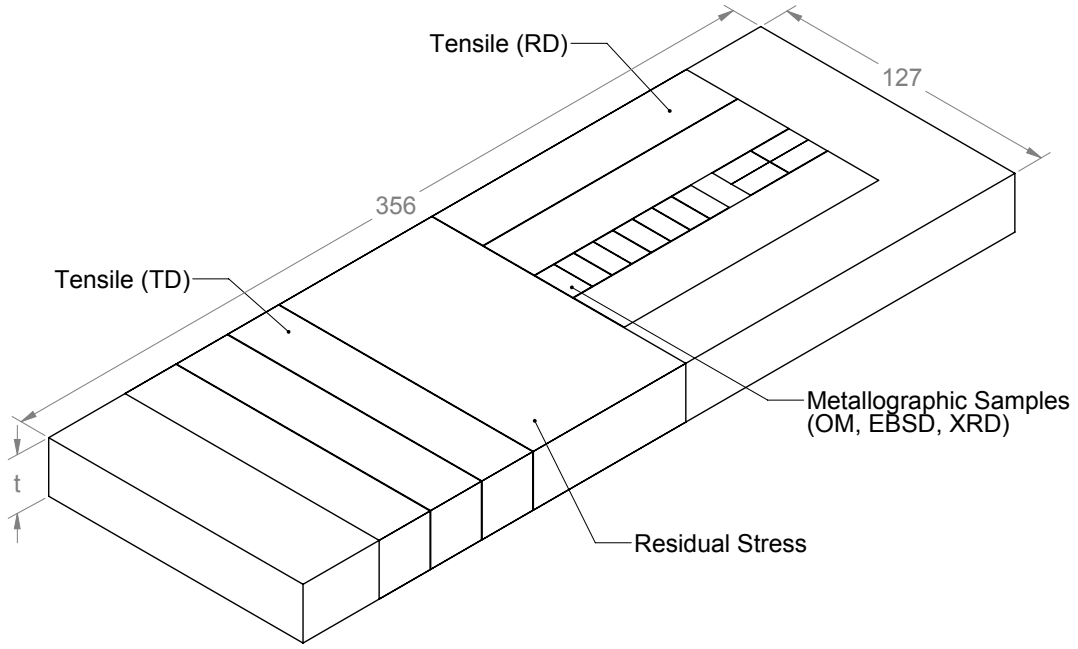

Figure 1: Layout of test specimens in a typical plate. Four round tensile samples (two in the RD, two in the TD) were tested in tensile testing for each plate. Several metallographic samples in the center of the plate are removed for optical microscopy, X-ray diffraction, electron backscatter diffraction study. A large section in the center of the plate is reserved for residual stress measurements. All units in mm.

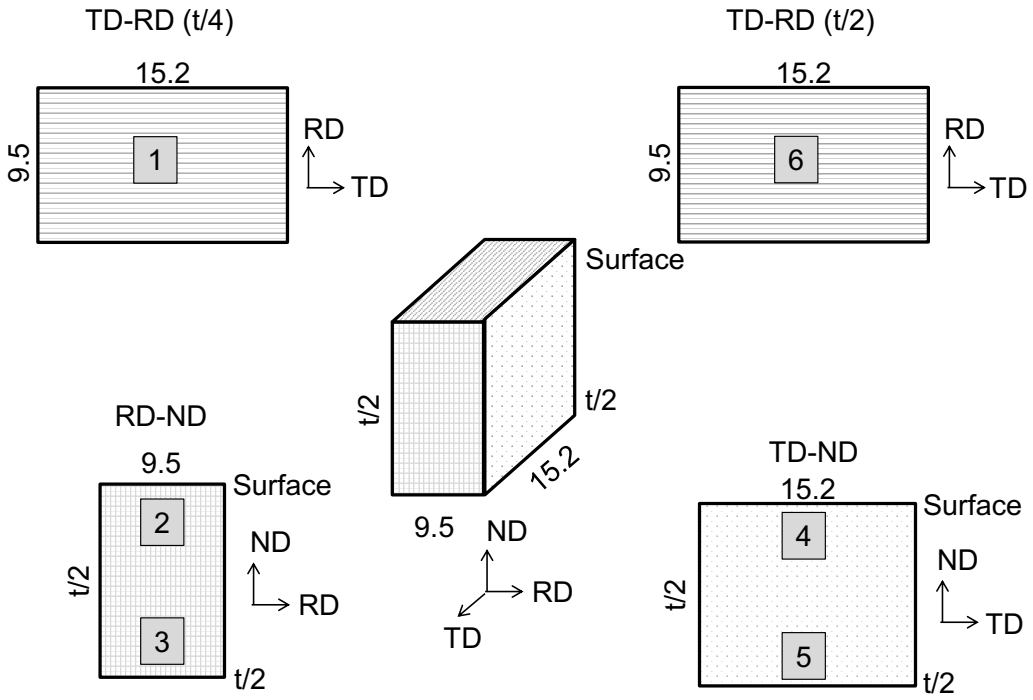

Figure 2: Sample geometry and approximate scan locations for EBSD analysis. Four thin samples are removed from a sample of comparable size to OM samples. All dimensions are in mm; thin samples have thickness of 1 mm. Figure not to scale.

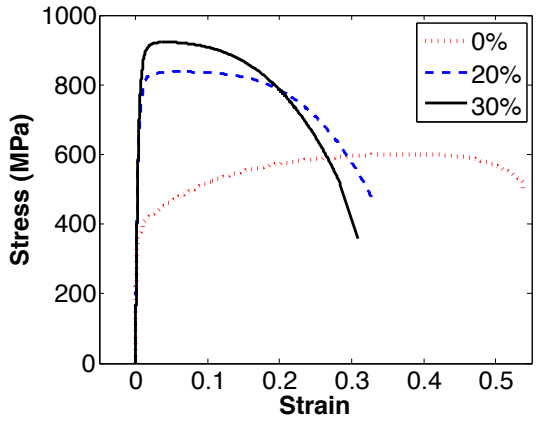

Figure 3: Engineering Stress-strain curves generated from tensile testing for samples in the 0%, 20%, and 30% CW conditions in the RD. Strain-hardening is readily apparent.

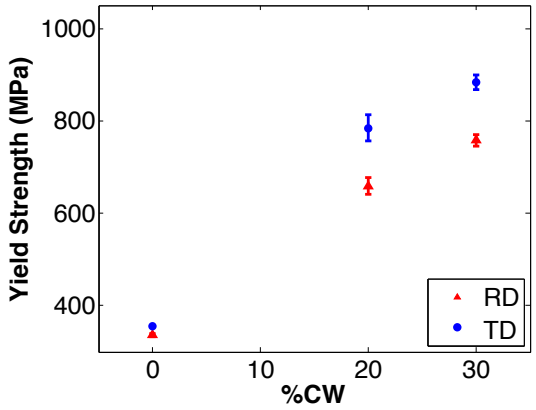

Figure 4: Directional anisotropy and dependence of yield strength on CW condition calculated from tensile testing. Error bars are one standard deviation.

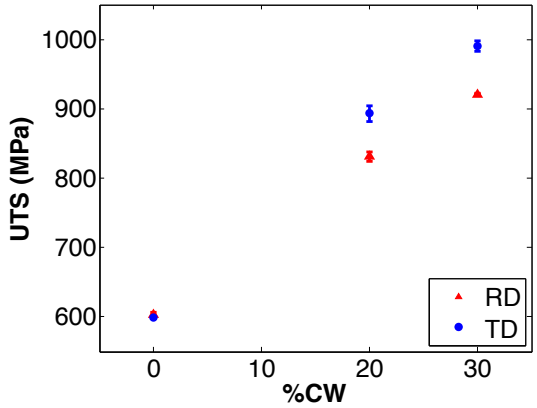

Figure 5: Directional anisotropy and dependence of ultimate tensile strength on CW condition calculated from tensile testing. Error bars are one standard deviation.

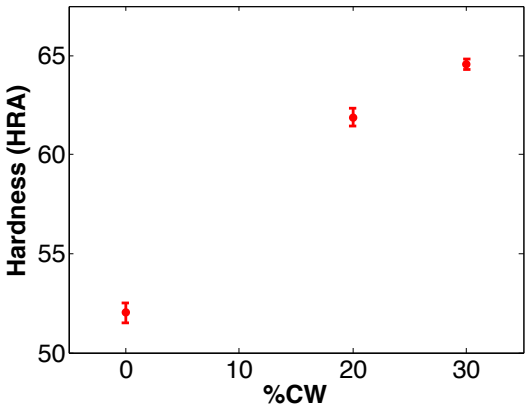

Figure 6: Rockwell hardness (converted A scale) as a function of CW condition. Error bars are one standard deviation.

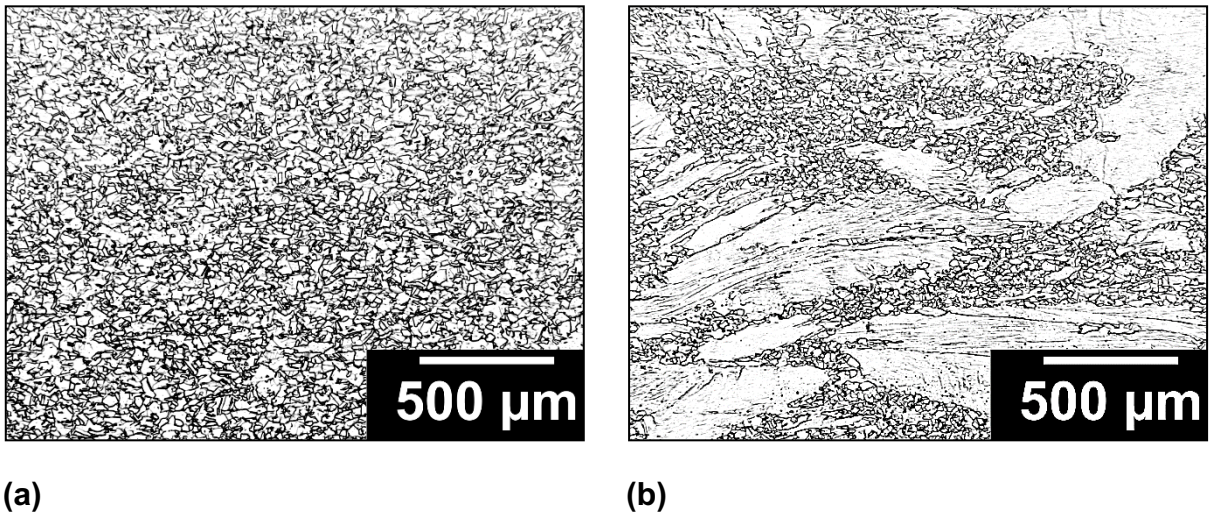

Figure 7: Optical Micrographs of 0% CW condition at 50x magnification showing through-thickness microstructural variation: (a) mid-thickness (b) bottom edge adjacent to the surface

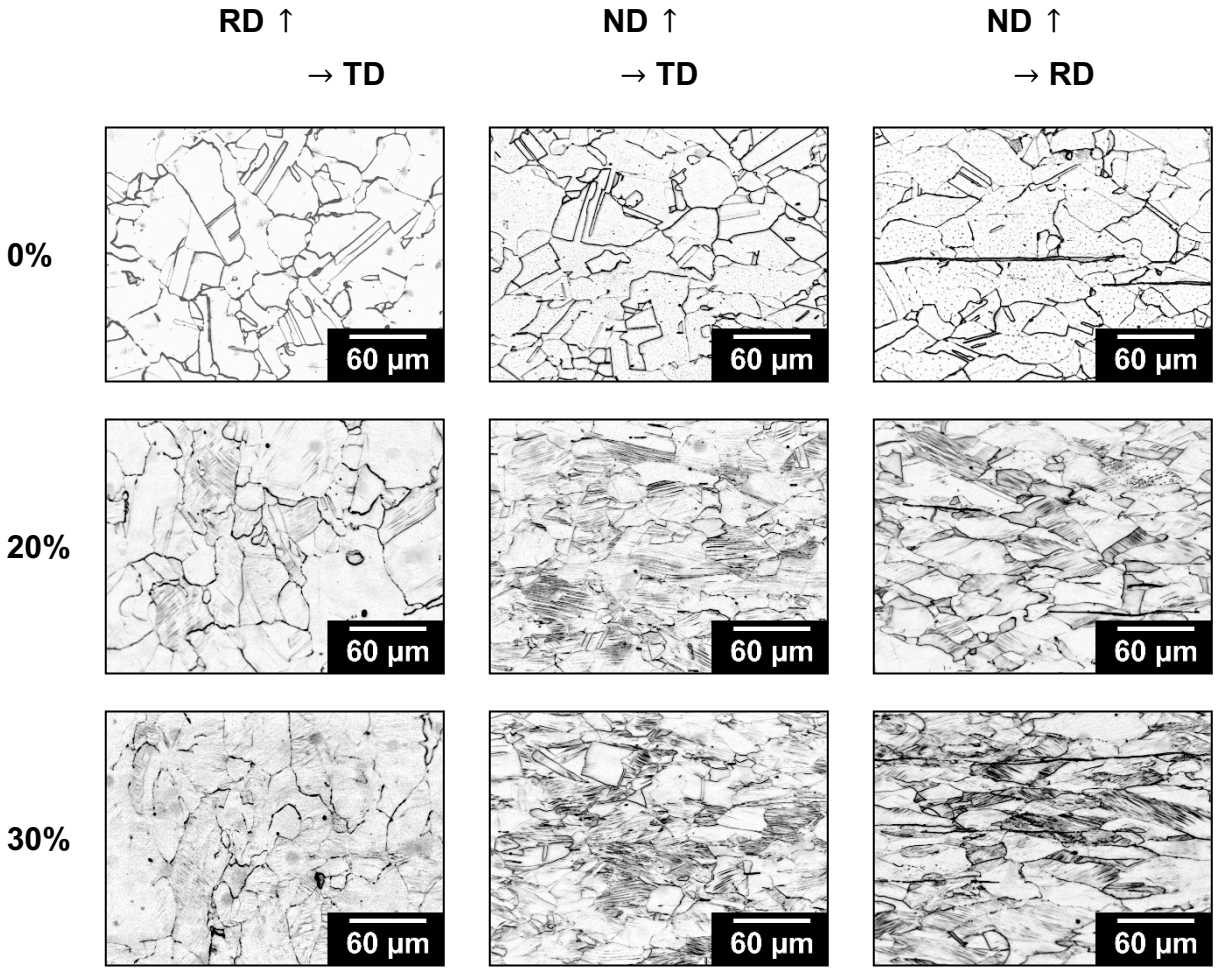

Figure 8: Etched micrographs showing deformation after rolling (elongating grains in RD) deformation twins (darkened areas within grains in 20% & 30% conditions), and ferrite stringers (black lines parallel to RD).

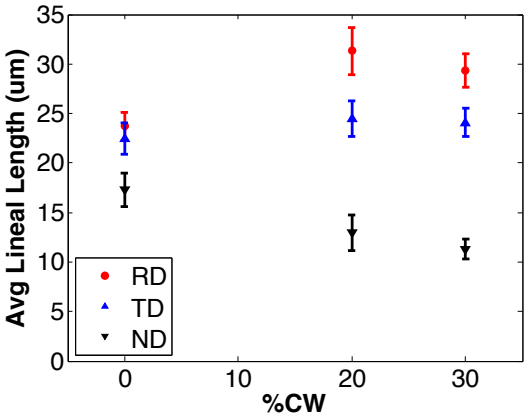

Figure 9: Average lineal lengths in each orthogonal direction as a function of CW condition showing that grain sizes follow macro geometric deformation of the plate

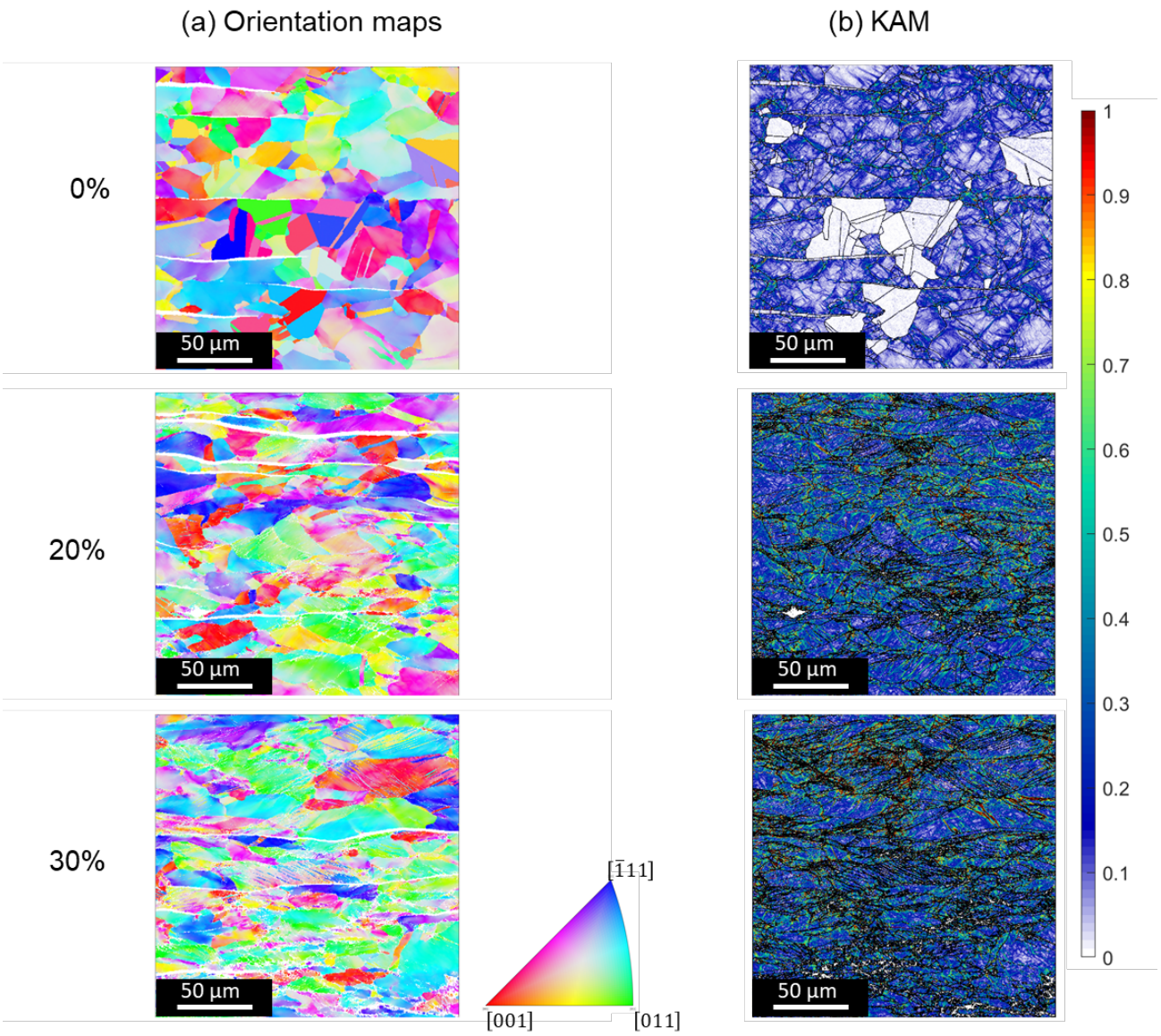

Figure 10: EBSD data for 0%, 20% and 30% RD-ND (mid-thickness) scan: (a) orientation map; and (b) KAM.. Ferrite stringers (horizontal strings), recrystallized grains (blue), and non-recrystallized grains (showing higher internal misorientation) are visible. KAM scale bar in degrees.

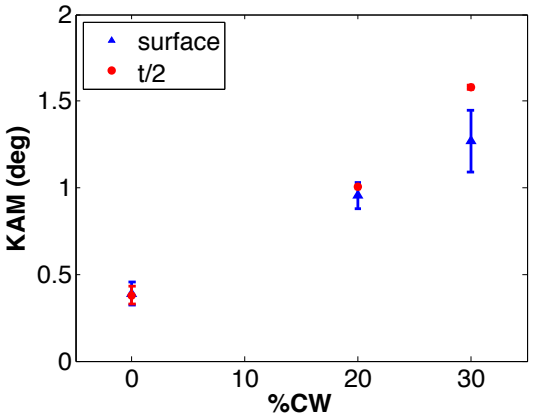

Figure 11: KAM as a function of CW condition for several scans. Results for both near-surface and bulk material are included.

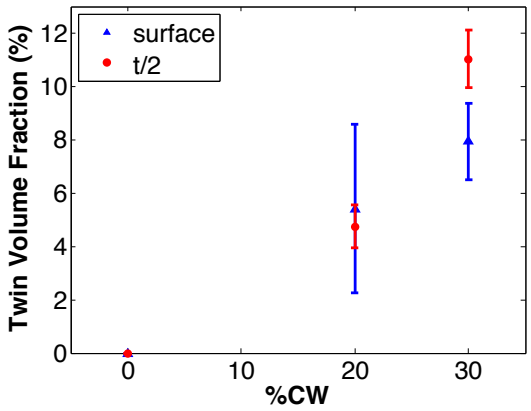

Figure 12: Deformation twin volume fraction as a function of CW condition for several scans. Results for both surface and bulk material are included.

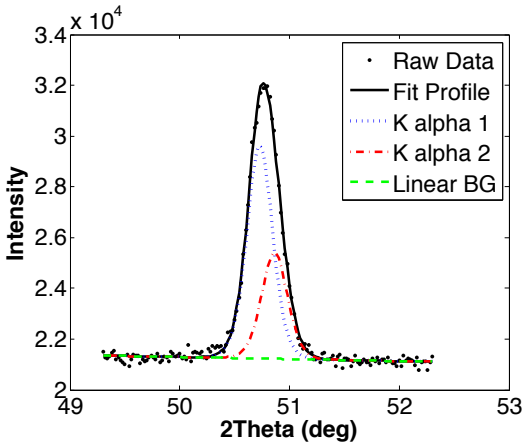

Figure 13: Peak 200 Pearson VII function fit to experimental XRD data showing contributions from $K\alpha_1$ $K\alpha_2$, and linear background components. Sample is 0% CW condition, RD-ND plane.

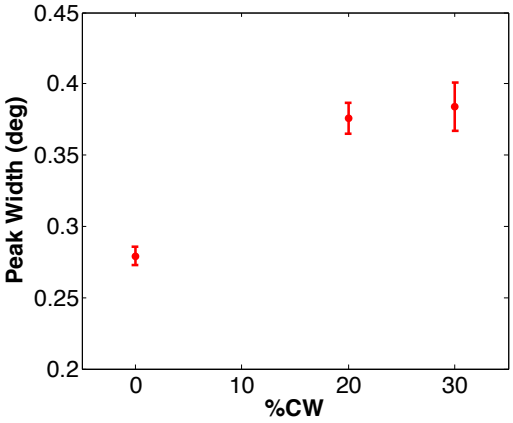

Figure 14: XRD peak width (FWHM) averaged over all nine samples per each CW condition. Error bars are one standard deviation

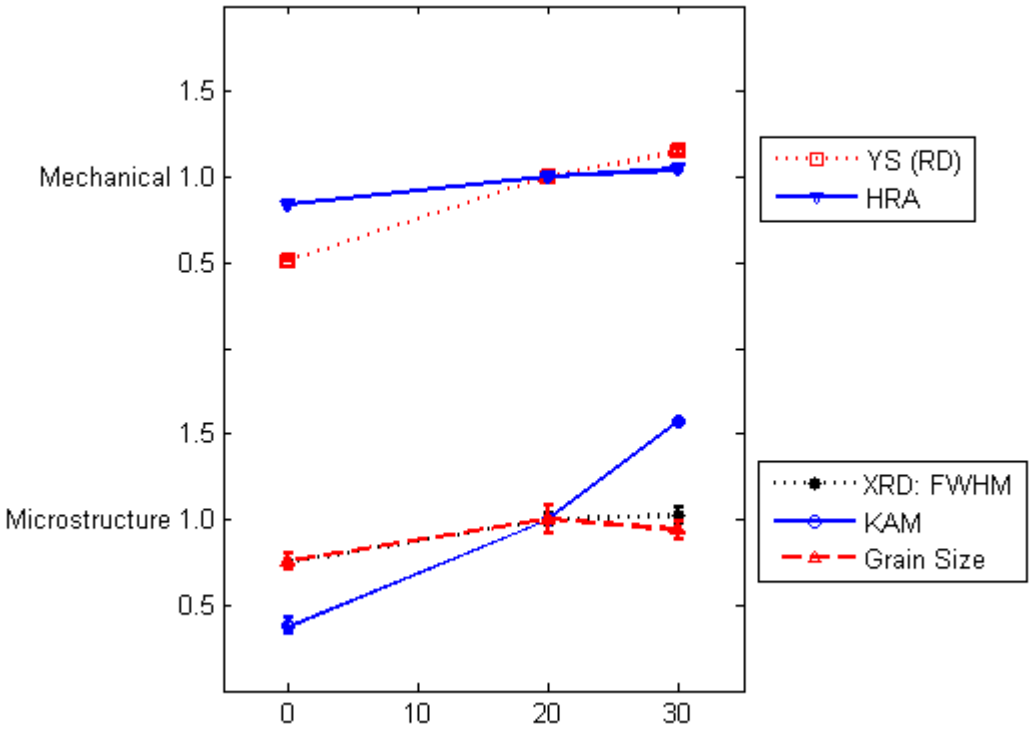

Figure 15: CW assessment methods normalized to 20% values

9 REFERENCES

[1] Shen, R.R., Review of Cold Work on Stress Corrosion Cracking of Alloy 690. Royal Institute of Technology.

[2] Electric Power Research Institute, Materials Reliability Program: PWR internals Material Aging Degradation Mechanism Screening and Threshold Values (MPR-175). 2005, EPRI: Palo Alto, CA.

[3] Electric Power Research Institute, Materials Reliability Program: Screening, Categorization, and Ranking of Reactor Internals Components for Westinghouse and Combustion Engineering PWR Design (MRP-191). 2006, EPRI: Palo Alto, CA.

[4] Electric Power Research Institute, Materials Reliability Program: Pressurized Water Reactor Internals Inspection and Evaluation Guidelines (MRP-227-A). 2011, EPRI: Palo Alto, CA.

[5] Moshier, W.C. and C.M. Brown, Effect of cold work and processing orientation on stress corrosion cracking behavior of alloy 600. Corrosion, 2000. 56(3): p. 307-320.

[6] Tice, D.R., et al., Crack growth testing on Cold Worked Alloy 690 in Primary Water Environment. 15th International Conference on Environmental Degradation of Materials in Nuclear Power Systems-Water Reactors, 2011: p. 71-87.

[7] Bruemmer, S., Olszta, M., Overman, N. and Toloczko, M., n.d., "Microstructural Effects on Stress Corrosion Crack Growth in Cold-Worked Alloy 690 Tubing and Plate Materials", ML13220A047, NRC: Pacific Northwest National Laboratory, Richland, WA.

[8] Program on Technology Innovation: Proceedings-2007 AECL/COG/EPRI Workshop on Cold Work in Iron- and Nickel-Base Alloys Exposed to High Temperature Water Environments: June 3-8, 2007, Mississauga, Ontario. 2008, EPRI, Palo Alto, CA, AECL, Mississauga, ON and COG,Toronto, ON.

[9] Electric Power Research Institute, Stress Corrosion Cracking Initiation Model for Stainless Steel and Nickel Alloys: Effects of Cold Work. 2009: EPRI, Palo Alto, CA.

[10] Huang, J.X., X.N. Ye, and Z. Xu, Effect of Cold Rolling on Microstructure and Mechanical Properties of AISI 301LN Metastable Austenitic Stainless Steels. Journal of Iron and Steel Research International, 2012. 19(10): p. 59-63.

[11] Nuclear corrosion science and engineering. Woodhead Publishing Series in Energy. 2012, Cambridge: Woodhead Publishing Ltd.

[12] Chopra, O., Soppet, W., and Shack, W., 2001, "Effects of Alloy Chemistry, Cold Work, and Water Chemistry on Corrosion Fatigue and Stress Corrosion Cracking of Nickel Alloys and Welds", NUREG/CR-6721, NRC, Washington D.C.

[13] Electric Power Research Institute, Materials Reliability Program: Resistance of Alloys 690, 52 and 152 to Primary Water Stress Corrosion Cracking (MRP-237, Rev. 1): Summary of Findings From Completed and Ongoing Test Programs Since 2004. 2008: EPRI, Palo Alto, CA.

[14] Andresen, P.L., M.M. Morra, and K. Ahluwalia, Scc of Alloy 690 and Its Weld Metals. 15th International Conference on Environmental Degradation of Materials in Nuclear Power Systems-Water Reactors, 2011: p. 161-176.

[15] Alexandreanu, B., Yang, Y., Chen, Y., and Shack, W., 2012, "Stress Corrosion Cracking in Nickel-Base Alloys 690 and 152 Weld in Simulated PWR Environment-2009", NUREG/CR-7137, Argonne National Laboratory, US Nuclear Regulatory Commision, Washington D.C.

[16] Fournier, L.e.a. Primary Water Stress Corrosion Cracking Resistance of Alloy 690 Heat Affected Zones of Butt Welds. in Fontevraud 8 - Contribution of Materials Investigations and Operating Experience to LWRs' Safety, Performance and Reliability. 2014. Avignon, France.

[17] Seiya Yamazaki, Z.L., Yuzuru Ito, Yoichi Takeda, Tetsuo Shoji, The effect of prior deformation on stress corrosion cracking growth rates of Alloy 600 materials in a simulated pressurized water reactor primary water. Corrosion Science, 2008. 50: p. 835-846.

[18] Kumagai, M., M. Imafuku, and S. Ohya, Microstructural Features of Cold-Rolled Carbon Steel Evaluated by X-ray Diffraction Line Profile Analysis and Their Correlation with Mechanical Properties. Isij International, 2014. 54(1): p. 206-211.

[19] Sakakibara, Y. and Nakayama, G., 2011, "The Effect of Cold Work on Microstructure and SCC Susceptibility in Simulated BWR Environment for Non-Sensitized Stainless Steels", 15th International Conference on Environmental Degradation of Materials in Nuclear Power Systems- Water Reactors, pp. 425-437..

[20] Lozano-Perez, S., Yamada, T., Terachi, T., Schroder, M., English, C., Smith, G., Grovenor, B., and Eyre, B., 2009, "Multi-Scale Characterization of Stress Corrosion Cracking, of Cold-Worked Stainless Steels and the Influence of Cr Content", Acta Materialia, 57, pp.5361-5381.

[21] Skuratov, D., Ratis, Y., Slezneva, I., Perez, J., Cordoba, P., and Urchueguia, J., 2007, "Mathematical Modelling and Analytical Solution for Workpiece Temperature in Grinding", Applied Mathematical Modelling, 31, pp.1039-1047.

[22] Turnbull, A., Mingard, K., Lord, J., Roebuck, B., Tice, D., Mottershead, K., Fairweather, N., and Bradbury, A., 2011, "Sensitivity of Stress Corrosion Cracking of Stainless Steel to Surface Machining and Grinding Procedure", Corrosion Science, 53(10), pp. 3398-3415.

[23] McGuire, M.F., Stainless Steels for Design Engineers. 2008: ASM International.

[24] ASTM Standard E8/E8M, Standard Test Methods for Tension Testing of Metallic Materials. 2013, ASTM International: West Conshohocken, PA.

[25] ASTM Standard E18, Standard Test Methods for Rockwell Hardness of Metallic Materials. 2014, ASTM International: West Conshohocken, PA.

[26] ASTM Standard E140, Standard Hardness Conversion Tables for Metals Relationship Among Brinell Hardness, Vickers Hardness, Rockwell Hardness, Superficial Hardness, Knoop Hardness, Scleroscope Hardness, and Leeb Hardness. 2012, ASTM International: West Conshohocken, PA.

[27] ASTM Standard E407, Standard Practice for Microetching Metals and Alloys. 2007, ASTM International: West Conshohocken, PA.

[28] ASTM Standard E112, Standard Test Methods for Determining Average Grain Size. 2013, ASTM International: West Conshohocken, PA.

[29] Prevéy, P.S., The measurement of subsurface residual stress and cold work distributions in nickel base alloys. Residual Stress in Design, Process & Materials Selections, ed. WB Young, Metals Park, OH: Am. Soc. For Metals, 1987: p. 11-19.

[30] Ji, V., Zhang, Y. and Chen, C., 2000, "The Non-Destructive Estimation of the Superficial Mechanical Properties of Components in the Inconel 600 Alloy by X-Ray Diffraction Peak Width", Surface and Coatings Technology, 130(1), pp. 95-99.

[31] Murugesan, S., Kuppusami, P., Mohandas, E., and Vijayalakshmi, M., 2012, "X-Ray Diffraction Rietveld Analysis of Cold Worked Austenitic Stainless Steel", Materials Letters, 67(1), pp. 173-176.

[32] Muransky, O., Balogh, L., Tran, M., Hamelin, C.J., Park, J.-S., Daymond, M.R.,"On the measurement of dislocations and dislocation substructures using EBSD and HRSD techniques", Acta Materialia 175 (2019), p. 297-313

[33] Mirzadeh, H., Cabrera, J., Najafizadeh, A., and Calvillo, P., 2012, "EBSD Study of a Hot Deformed Austenitic Stainless Steel", Materials Science and Engineering: A, 538, pp. 236-245.